Technical University of Denmark

DTU

Dimensional behavior of Ni-YSZ composites during redox cycling

Pihlatie, Mikko; Kaiser, Andreas; Larsen, Peter Halvor; Mogensen, Mogens Bjerg

DTU Library
Technical Information Center of Denmark

Dimensional Behavior of Ni–YSZ Composites during Redox Cycling

M. Pihlatie,[a,b,c,z] A. Kaiser,[a] P. H. Larsen,[a] and M. Mogensen[a,*]

[a]*Risoe National Laboratory for Sustainable Energy, Department of Fuel Cells and Solid State Chemistry, Technical University of Denmark, DK-4000 Roskilde, Denmark*
[b]*Department of Engineering Physics, Helsinki University of Technology, Espoo, Finland*

The dimensional behavior of Ni–yttria-stabilized zirconia (YSZ) cermets during redox cycling was tested in dilatometry within the temperature range 600–1000°C. The effect of humidity on redox stability was investigated at intermediate and low temperatures. We show that both the sintering of nickel depending on temperature of the initial reduction and the operating conditions, and the temperature of reoxidation are very important for the size of the dimensional change. Cumulative redox strain (CRS) is shown to be correlated with temperature. Measured maximum CRS after three redox cycles varies within 0.25–3.2% dL/L in dry gas and respective temperature range of 600–1000°C. A high degree of redox reversibility was reached at low temperature, however, reversibility is lost at elevated temperatures. We found that at 850°C, 6% steam and a very high p_{H_2O}/p_{H_2} ratio is detrimental for redox stability, whereas at 600°C no negative effect was observed. Pre-reduction at 1100 instead of 800°C more than doubled redox strain on reoxidation at 800°C. For samples similarly pre-reduced at 1000°C, lowering the reoxidation temperature from 1000 to 750°C or below reduces the redox strain to less than half.
© 2008 The Electrochemical Society. [DOI: 10.1149/1.3046121] All rights reserved.

The anode-supported solid oxide fuel cell (SOFC) concept based on Ni–yttria-stabilized zirconia (YSZ) anode materials is under intensive research and development. While new materials are being sought, e.g., fully ceramic anodes capable of operating at lower temperatures, the nickel-based ceramic–metal composite (cermet) anode is so far the reference to which the new anodes will be compared. So far no nickel-free anodes have been proven superior in long-term operation at technologically relevant sizes up to the stack and system level. In spite of this, some problems are associated with the Ni–YSZ electrode. The conductivity of a Ni–YSZ composite is known to degrade with time under operation at high temperature due to the growth of Ni grains, whereas the ceramic backbone remains largely unaltered.[1,2] The sintering of the Ni network may result in performance degradation through loss of electrical conductivity of the anode support (current collection). It is known from catalysis with nanosized Ni on ceramic beds that both temperature and humidity (the H_2O/H_2 ratio) enhance Ni particle growth; the effect of steam arises from the formation and mobility of the Ni_2–OH species.[3,4] The mobility also of micrometer-sized Ni embedded in the porous YSZ backbone is dependent on operation conditions and increases with temperature. Sintering of Ni has been proposed as one of the mechanisms behind the so-called redox instability.[5]

As discussed, e.g., in a recent review by Sarantaridis and Atkinson,[6] the difficulty related to redox stability of Ni-based SOFCs arises from the large volumetric change in the Ni–NiO reduction–oxidation reaction combined with the fact that the Ni rearranges itself in a way that the existing porosity in the composite no longer can accommodate the expansion upon reoxidation. The manufacturing route brings the cermet-supported SOFC into an oxidized state, typically containing 45–60 wt % NiO and YSZ for balance. When a cell is taken into operation, the NiO is reduced and it shrinks 41% $\Delta V/V$. The molar volumes of Ni and NiO are 6.59 and 11.20 cm³/mol, respectively.[6] As a result, new porosity is created. If the anode compartment is again subjected to oxidizing atmosphere during the operation of the cell at high temperature, the Ni will readily reoxidize to NiO. The reoxidation of Ni brings about a 69% dV/V expansion and can be devastating to the SOFC. Several papers from different groups have already been presented on the redox behavior of Ni–YSZ composites, e.g., Ref. 5 and 7-11. In a model proposed by Klemensø and Mogensen,[12] the irreversible redox ex-

pansion of Ni would gradually create first micro- and later macrodamage in the ceramic backbone in the form of mechanical degradation, in the worst case leading to mechanical disruption of the composite. This aspect will be further discussed elsewhere.

The problem of redox stability can be tackled using different approaches, for example, modifying the cell design (e.g., electrolyte vs anode-supported planar SOFC), materials selection (e.g., Ni-based vs fully ceramic or metal-supported SOFC), or by defining safe operation regimes and system controls of a selected design or composition (knowledge of so-called external parameters and SOFC system logics). The reoxidation of the anode-supported cell can lead to (*i*) degradation and disruption of the anode support itself, or (*ii*) cracking of the electrolyte in a cell structure due to excessive macroscopic expansion of the anode support. Two requirements for a redox-improved anode-supported Ni–YSZ half-cell can be identified:

1. Based on mechanical modeling, the maximum allowable expansion of the anode support does not exceed 0.1–0.2% dL/L.[13-15] As larger expansions create tension forces that tend to crack the electrolyte, this cumulative strain level should not be exceeded. For development work, 0.1% maximum cumulative redox strain (CRS_{max}) is chosen as the target level.

2. During redox cycles the behavior of the composite should be reversible, that is, after the reoxidation cycle the bulk dimension should return to the original. An irreversible expansion will inevitably limit the number of allowable redox cycles and lead to violation of the first requirement.

This paper describes dimensional changes in Ni–YSZ composites under redox cycling in a wide range of operation conditions. We aim to address the "internal" processes of importance that take place in the composite. Part of the high–temperature data of the present paper have previously been published in Ref. 16.

Experimental

Ceramic processing.— The samples tested were manufactured from commercial NiO and 3YSZ powders using standard ceramic processing techniques and equipment. The solids composition of the samples was 53–56 wt % NiO and 44–47 wt % YSZ. The powders were ballmilled in ethanol-based slurries using dispersants and organic binders. The tested samples were similar to the anode supports
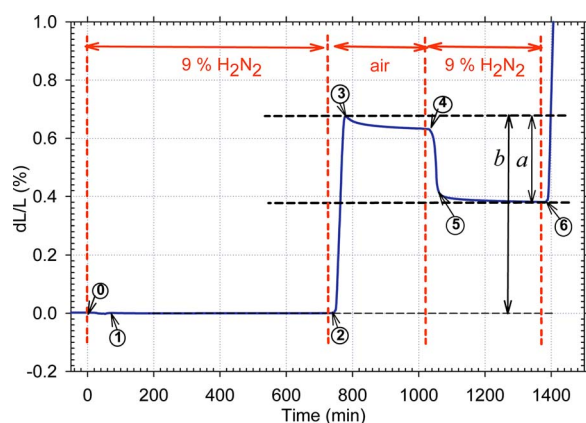
Figure 1. (Color online) The gas change sequence as a function of time during isothermal redox cycling dilatometry, dL/L$_o$, shown by the solid line. Heat-up occurred under air and during negative time (not shown); the initial reduction commences at $t = 0$. Between each air/9% H$_2$ change a short flush of N$_2$ was implemented. DRR is the fraction of reoxidation strain recovered during the following re-reduction, defined as a/b. The CRS and DRR analysis is based on strain at the indicated numbered points (0–6 in the present figure) during redox cycling.

of the state-of-the-art Risoe-TOFC^d cells.[17,18] Two different slurries following the same processing route and parameters were tape-cast into green tapes, later referred to as A and B. Although the processing route of slurries A and B was the same, small differences in the resulting composites were possible due to, e.g., particle size distributions or sintering conditions. Slurry B was cast in two different thicknesses. After sintering at 1300–1400°C, the green tapes yielded ceramic plates of 0.4–0.7 mm thickness. These thicknesses were necessary in order to reduce the risk of bending of the samples while testing at high temperatures and under redox strains. Prior to sintering, the green tapes were cut into a number of sibling pieces. The as-sintered sizes of the samples were on the order of 5×24 mm. The as-sintered open porosities of the samples were measured by mercury intrusion porosimetry using a Micromeritics instrument and were 15–16% for tape A and 12–13% for tape B. The resulting porosities in the reduced state were on the order of 35–40%. Total porosities were estimated for some samples by geometrical volume, sample weight, and the theoretical density. The obtained total porosities from geometrical measurements were 21–25%, but due to uncertainties related to the small sample, should only be taken as an approximate upper bound of total porosity.

Dilatometer procedures.— A series of redox tests of the sintered cermets was carried out using a Netzsch 402 CD differential dilatometer equipped with a gas control unit capable of programmed mixing of up to three different gases. The heating rate used was 3–4°C/min. After a hold of about 1 h in air at the test temperature, the gas was switched to diluted hydrogen with a 20 min flush of N$_2$ in between. Furthermore, a p_{O_2} sensor running at a constant temperature was connected downstream in some of the tests to measure the oxygen partial pressure in the gas exiting the dilatometer. The p_{O_2} at the test temperature was calculated using the Nernst equation and hydrogen-steam reaction equilibrium constants at the test and sensor temperatures. Sibling samples of the thin Ni–YSZ cermets were exposed in dilatometry to reduction–oxidation cycles at temperatures between 600 and 1000°C. The gas change sequence is illustrated in Fig. 1, where the first reoxidation cycle at 850°C is marked; a change of gas was always preceded by a short N$_2$ flush. The redox cycling was in most tests carried out by varying between

artificial air (20% O$_2$ and 80% N$_2$) and dry diluted hydrogen (mixture of 9% H$_2$ and 91% N$_2$), with the said flush of N$_2$ in between.

In real anode operation, water vapor will always be present. Humidity is believed to accelerate degradation due to sintering of nickel in microcomposites, possibly through changes in surface diffusivity of Ni on nickel grains,[19,20] this effect is also known from nanocatalysis.[3,4] Therefore, four test cases were run where the p_{O_2} was varied during the test by combining varying flows of diluted hydrogen and nitrogen with a small flow of air. Three tests were carried out isothermally at 850°C and the fourth one at 600°C. The gas change sequences in the four redox tests with humidity were implemented as follows. In the first test, the initial reduction and re-reductions after each redox cycle were carried out in dry 9% H$_2$; at 850°C the oxygen partial pressure was typically $p_{O_2} \approx 10^{-20}$. The reoxidation sequences started by a 2 h humid gas flow of 6, 51, and 46 mL/min of air, 9% H$_2$ diluted in N$_2$ and N$_2$, respectively. The air flow of 6 mL/min equals an O$_2$ flow of 1.2 mL/min. The planned gas composition in this 2 h period was approximately 94.4% N$_2$, 2.7% H$_2$, 3.0% H$_2$O, $p_{O_2} \approx 6.5 \times 10^{-18}$, and a p_{H_2O}/p_{H_2} of 1.10. After 2 h under the humid conditions the gas was switched first to a mixture of 80% N$_2$ and 20% air ($\log[p_{O_2}] \approx -1.4$) for 2 h and then to dry air. In the remaining three tests the humidified or dry oxidizing conditions prevailed through the entire duration of the redox cycles, until terminated by a N$_2$ flush and re-reduction. In the second test, the ratio between 9% H$_2$ in N$_2$ and N$_2$ was varied between redox cycles by stepwise reducing the flow of diluted H$_2$ (e.g., 55 → 45 → 40 → 35 mL/min 9% H$_2$ diluted in N$_2$), and respectively increasing flow of N$_2$ in order to keep the total gas flow at 100 mL/min the air flow was kept constant at 6 mL/min. The planned p_{H_2O}/p_{H_2} for the four flows of diluted H$_2$ are 1.0, 1.4, 1.9, and 2.9, respectively, and the p_{O_2} increases stepwise in successive redox cycles. The re-reductions were always carried out in dry, diluted 9% H$_2$. In the third test, four redox cycles were implemented and the corresponding 9% H$_2$ flows in each of the cycles were 42, 38, 31, and 0 mL/min, with p_{H_2O}/p_{H_2} of 1.6, 2.2, 5.1, and undefined, respectively. For the fourth test at 600°C, five redox cycles were implemented with the corresponding 9% H$_2$ flows being 41, 40, 38, 36, and 31 mL/min and p_{H_2O}/p_{H_2} of 1.8, 1.9, 2.2, 2.9, and 5.1. At the test conditions, virtually all of the oxygen supplied will react with hydrogen to produce steam, and the planned p_{H_2O} was according to thermodynamic calculation between 3 and 3.4%. The tightness of the system and variations in actual gas flow give rise to uncertainty in humidity. For example, variation of 1 mL/min in the air flow from the nominal 6 mL/min corresponds to about $\pm 0.7\%$ points in p_{H_2O}. The actual gas composition that resulted during the experiments is discussed in the Results section.

In dilatometry, the push rod exerted a longitudinal force of 30 cN on the sample during the measurement, corresponding to about 0.8–1.8 kPa depending on the sample cross-sectional area. The total gas flow during the tests was 50 and 100 mL/min during the tests reported in the following subsections. After testing, both fracture surfaces and polished cross sections of several samples were examined in a JEOL low-vacuum scanning electron microscope (SEM) or Zeiss Supra field emission SEM. The accuracy of the differential dilatometer used is very good and the temperature control accurate within about 0.5°C. The biggest source of uncertainty in the results arises from possible sample-to-sample variations in, e.g., porosity. Such variations were, for example, observed between tapes A and B and they could arise from small differences between slurries or, e.g., slightly different sintering temperatures. However, in each subset of experiments where the dimensional response under different conditions is compared, the samples always stem from the same tape. Reproducibility of measurements using samples from the same tape and sintering batch was good.
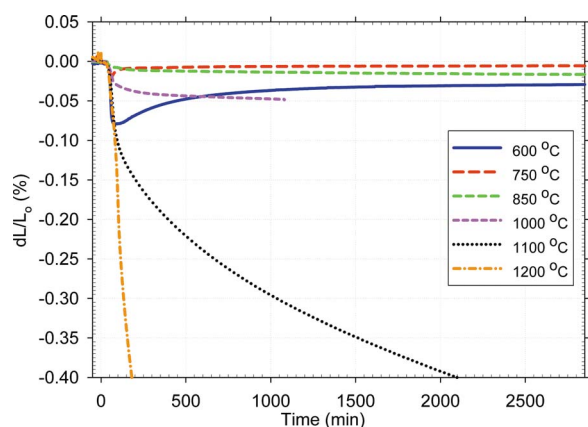
Figure 2. (Color online) Relative sample length change from the hot as-sintered state of NiO–YSZ composites as a function of time during isothermal reduction at different temperatures in dry 9% H_2 (diluted in N_2). The reduction commences at $t = 0$.
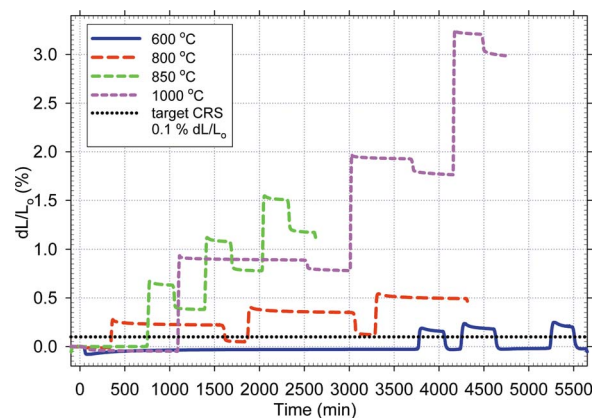

Figure 3. (Color online) Relative length change of Ni–YSZ composites as a function of time during three isothermal reoxidation cycles under dry conditions at different temperatures. The initial reduction takes place at $t = 0$, and the dL scale shows relative length change from the hot as-sintered state prior to the initial reduction.

Results

Unless otherwise stated in the sections that follow, the scales in all graphs have $t = 0$ when the initial reduction commences. The zero point on the relative dL/L_o scale corresponds to the hot state prior to the initial reduction; thermal expansion during heating has been deducted. The length change is calculated relative to the as-sintered cold sample length. For strain as a function of redox cycling we have used the term, the cumulative redox strain (CRS).

Initial reduction.— The dimensional response of the NiO–YSZ composite to reduction was investigated at temperatures from 600 to 1200°C. Isothermal dilatometry was carried out for up to 48 h under a reducing atmosphere in order to study the dimensional changes. Upon the first reduction of the composite, clear differences

in dimensional response were measured depending on reduction temperature, as displayed in Fig. 2 and tabulated in Table I ($n = 0$, $CRS_{reduced}$). The tested samples were from tape A.

Redox cycling in dry gas.— Results from the isothermal dilatometry are shown in Fig. 3. Three redox cycles were carried out isothermally at each temperature for samples from tape A. The expansion strains upon reoxidation strongly depend on conditions with varying degree of contraction back toward the initial length taking place upon the re-reductions. CRS as a function of redox cycles at the different isothermal temperatures is summarized in Table I, where CRS_{max} is the maximum strain measured during a redox cycle, and $CRS_{reduced}$ is the measured strain at the end of the reducing step following that redox cycle.

A SEM backscattered electron image (BEI) from a polished cross section of an as-sintered NiO–YSZ composite is shown in Fig. 4. YSZ appears light gray, NiO is dark gray, and porosity is black. BEI images from polished cross sections after reduction for 48 h at 600°C are shown in Fig. 5A and after three redox cycles in Fig. 5B; now there is no contrast between metallic Ni and YSZ due to a similar electron backscatter coefficient. For comparison, the polished surfaces after reduction for 13 h and three times redox cycling at 1000°C are displayed in Fig. 6A and B, respectively. Porosity of the reduced samples has increased compared to the as-sintered state due to Ni reduction. The microstructure after low-temperature re-

Table I. CRS and DRR parameters from isothermal dilatometry experiments. CRS_{max} is the maximum strain measured during a redox cycle, and $CRS_{reduced}$ is the measured strain at the end of the reducing step following that redox cycle ($n = 0$ equals the as-sintered state). DRR is the fraction of expansion strain that is recovered upon re-reduction following each reoxidation.

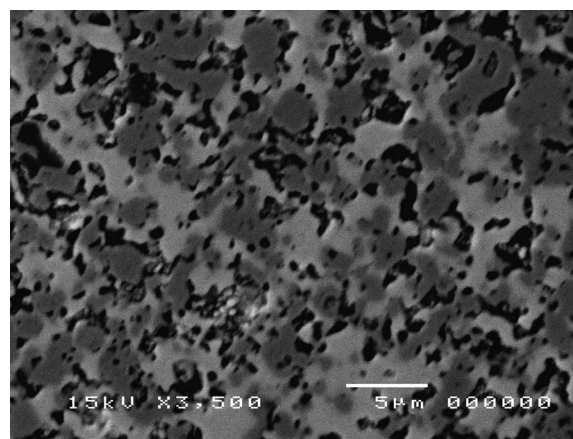| Test case	n of redox cycle	CRS_{max}	$CRS_{reduced}$	DRR
600°C (Fig. 3)	0	0	−0.08	—
	1	0.19	−0.02	0.98
	2	0.24	−0.02	0.98
	3	0.25	−0.02	1.01
800°C (Fig. 3)	0	0	−0.01	—
	1	0.28	0.05	0.82
	2	0.40	0.12	0.79
	3	0.54	—	—
850°C (Fig. 3)	0	0	0.00	—
	1	0.68	0.38	0.44
	2	1.12	0.78	0.46
	3	1.55	1.17	0.49
1000°C (Fig. 3)	0	0	−0.02	—
	1	0.93	0.78	0.16
	2	1.97	1.76	0.17
	3	3.25	2.99	0.18
850°C humid (Fig. 7)	0	0	−0.01	—
	1	0.96	0.63	0.34
	2	1.79	1.41	0.33
	3	2.78	2.36	0.31

Figure 4. Backscattered electron image in SEM of a polished cross section of the as-sintered NiO–YSZ composite.
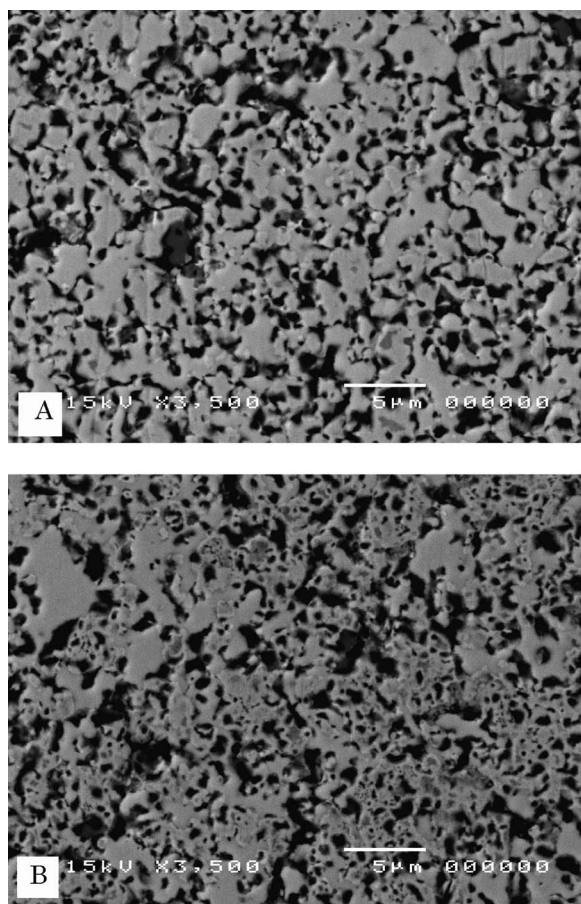
Figure 5. Polished SEM micrograph of the Ni–YSZ cermet reduced at 600°C (A) and the same material redox cycled three times at 600°C (B).
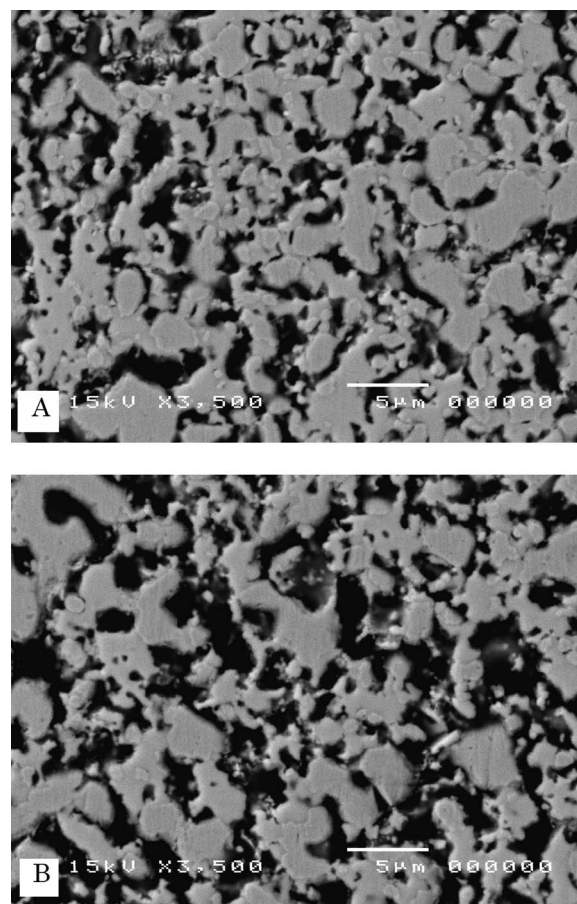

Figure 6. Polished SEM micrograph of Ni–YSZ cermet reduced at 1000°C (A) and the same material redox cycled three times at 1000°C (B).

duction has caused remarkably less growth of Ni grains than after high-temperature reduction, as can be observed by comparing Fig. 5A and 6A, where Fig. 5A clearly shows a finer microstructure. Redox cycling three times at 600°C (Fig. 5B) shows further refinement of the microstructure. The third reoxidation time during redox cycling at 600°C was 5 h and the subsequent re-reduction 3 h (Fig. 3). As will be evident from an upcoming paper on thermal analysis and also as reported in Ref. 8, these times were possibly insufficient for full oxidation or reduction. Figure 5B also shows creation of some new intragranular porosity in the Ni phase. This effect was also reported by, e.g., Sarantaridis[11] and is known from high-temperature oxidation of nickel.[21] After tests at 1000°C, the cermet shows increased grain and pore size after reduction (Fig. 6A). Microstructural damage and loss of contact between grains due to redox cycling can be observed in Fig. 6B; the sample was also macroscopically cracked.

Variation in p_{O_2}, p_{H_2}, and p_{H_2O}.— Three tests were executed at 850°C and a fourth one at 600°C to examine the effect of humidity and p_{O_2} on the dimensional redox behavior of Ni–YSZ cermets. The three tests at 850°C were done with samples from tape A and the test at 600°C using a sample from tape B. Figures 7-10 show the results from the isothermal dilatometry, where the measured oxygen partial pressures at the test temperature are given by the dashed lines. Results from the first test are shown in Fig. 7. The gas changes are illustrated by the vertical dashed lines separating the following steps: the time prior to I pertains to reduction in dry 9% H$_2$, followed by (I) humid reducing-oxidizing (air + N$_2$ + H$_2$); (II) air + N$_2$; (III) air; and (IV) humid oxidizing (air + N$_2$ + H$_2$). After IV the sample was re-reduced. When humidity is introduced during the

initial 2 h of the redox cycle (part I), the relative expansion upon subsequent reoxidation increases clearly from the dry air case (shown in Fig. 3; see Table I). During this 2 h period there is little bulk expansion in the sample although the p_{O_2} rises to $\sim 2 \times 10^{-4}$, which is above the oxidation threshold and much more than what was predicted using the nominal input gas flows, $p_{O_2} \approx 7 \times 10^{-18}$.
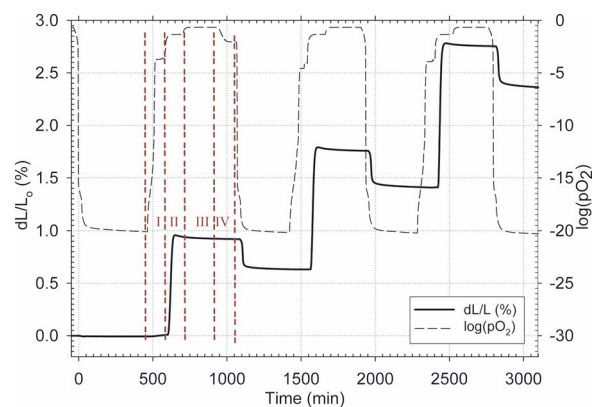

Figure 7. (Color online) Measured relative length change of a Ni–YSZ cermet and p_{O_2} of the atmosphere as a function of time. Redox cycling is carried out isothermally at 850°C with 6% steam introduced for 2 h (part I) prior to each reoxidation in dry air (parts II–III). The initial reduction commences at $t = 0$, and the dL scale shows relative length change from the hot as-sintered state prior to the initial reduction.

Figure 8. Relative length change vs time for Ni–YSZ cermet during isothermal dilatometry at 850°C with 6% humidity. An effect of p_{O_2} on strain is observed with little expansion emerging at $p_{O_2} \approx 5 \times 10^{-17}$, which is about 50 times higher than the equilibrium p_{O_2} for the Ni/NiO reaction at that temperature. The initial reduction commences at $t = 0$, and the dL scale shows relative length change from the hot as-sintered state prior to the initial reduction.
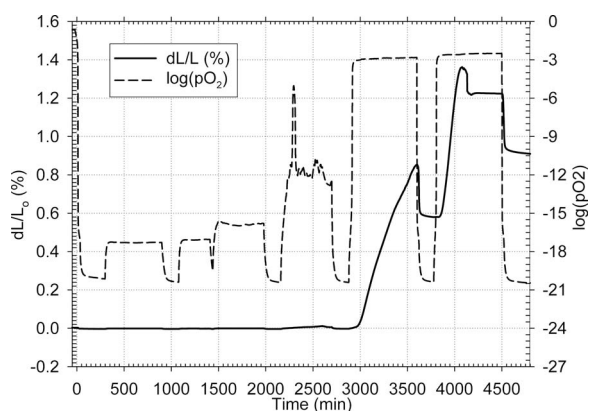

Figure 10. Relative length change vs time for Ni–YSZ cermet during isothermal dilatometry at 600°C with 6% humidity. The first expansion was measured at $t \approx 2700$ min with $\log[p_{O_2}] \approx -2.5$, but due to slow kinetics the oxidation was not completed. The last reoxidation at t $\approx$ 6400 min resulted in a peak CRS. The initial reduction commences at $t = 0$, and the dL scale shows relative length change from the hot as-sintered state prior to the initial reduction.

Based on the measured p_{O_2}, the gas composition during the 2 h period is $p_{H_2O} = 0.067$, $p_{H_2} = 1.3 \times 10^{-8}$, $p_{N_2} = 0.93$, $p_{O_2} \approx 1.5 \times 10^{-4}$, and $p_{H_2O}/p_{H_2} = 5.29 \times 10^6$.

The second test run with varying p_{O_2} levels is shown in Fig. 8. The final strain levels were not reached in the test shown in Fig. 8, as the gas was switched back to reducing before stabilization at $t \approx 3600$ min, and the sample bent upon the second reoxidation, about $t \approx 4100$ min. The spike in p_{O_2} at $t \approx 2300$ min is probably due to a transient in actual gas flow that was too short to initiate cermet expansion. The third test, shown in Fig. 9, was comprised of four redox cycles isothermally at 850°C using a thicker laminated sample. The maximum redox strain after three redox cycles in humid gas was 3.5%. Another redox cycle in dry air was started at $t \approx 14000$ min, and this increased CRS_{max} to 3.6%. Figure 10 displays results from the humid redox cycling test carried out at 600°C. The maximum redox strain is about 0.21% dL/L, which is close to what was measured during redox cycling in dry gas at the same temperature (0.19% after the first and 0.25% after the third reoxida-
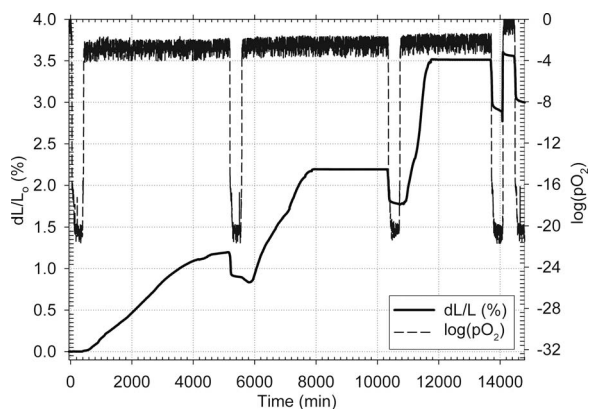

Figure 9. Relative length change vs time for Ni–YSZ cermet during isothermal dilatometry at 850°C with 6% humidity. Measured $\log[p_{O_2}]$ during the three first reoxidations were about −2.8, −2.5, and −2.3 for respective reoxidation times of approximately 500, 5500, and 10,500 min. Increase in p_{O_2} is reflected in the expansion rate. The fourth reoxidation at $t \approx 14,000$ min occurs in dry air. The initial reduction commences at $t = 0$, and the dL scale shows relative length change from the hot as-sintered state prior to the initial reduction.
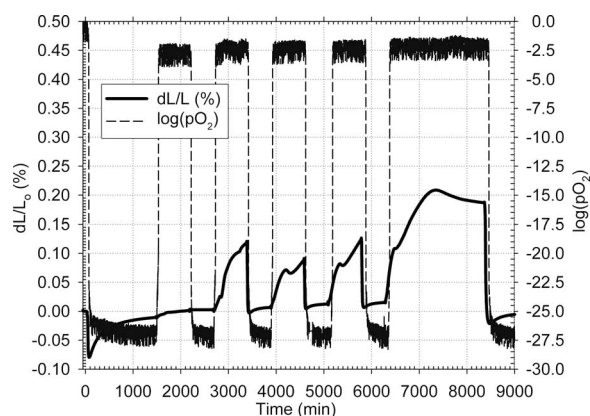
tion, see Table I). Calculation of the actual gas composition based on the p_{O_2} measurement indicates that the p_{H_2O} during the oxidation periods in Fig. 8 is about 6% and the corresponding p_{H_2O}/p_{H_2} is very high; the same holds for the gas composition in experiments shown in Fig. 9 and 10, except for the last reoxidation in Fig. 9, which was carried out in dry air. In other words, besides the system tightness, estimated to be about 0.002, the actual air flow was higher than the set value.

Effect of the initial reduction temperature.— The effect of temperature during the initial reduction on redox stability was investigated by reducing two cermets from tape A at two different temperatures. One sample (case 1) was reduced 4.5 h at 1100°C, taken down in temperature to 800°C for 25 h before the reoxidation. The other sample (case 2) was reduced 5.5 h at 800°C. After the initial reduction, both cermets were reoxidized at 800°C. By testing two sibling samples in this way the difference in redox strain can be ascribed to different Ni–YSZ microstructures due to sintering of nickel during operation under reducing conditions. The results of the tests are shown in Fig. 11. The dL/L$_o$ = 0 point for case 1 is prior to the reoxidation, and for case 2 before the initial reduction; the initial difference when reoxidation commences is about 0.01. The time scales were shifted so that the reoxidation takes place simultaneously; for case 2 the initial sample reduction occurs from $t = 0$, for case 1 during negative time (not shown). The maximum redox strain from the first redox cycle is 0.27% dL/L$_o$ for reduction at 800°C (the entire redox curve is shown in Fig. 3). In case 1 the measured bulk expansion upon reoxidation at 800°C is about double, 0.59%. The decrease of the dL/L curve at $t \approx 1400$ min and after is due to rereduction of the samples.

Effect of the reoxidation temperature.— The effect of the reoxidation temperature on redox stability was investigated by reducing Ni–YSZ samples 3 h at 1000°C and exposing them to air at different temperatures. The chosen reoxidation temperatures were 1000, 850, 750, and 600°C; after the initial reduction the samples were cooled to the reoxidation temperature. The samples were additionally stabilized for 1 h at the reoxidation temperature before the reoxidation. Samples prepared from tape B were used, though the sample tested at 850°C was thicker and sintered in a batch different from the other samples. When the initial reduction treatment of the samples was the same, the differences in redox strain response are in
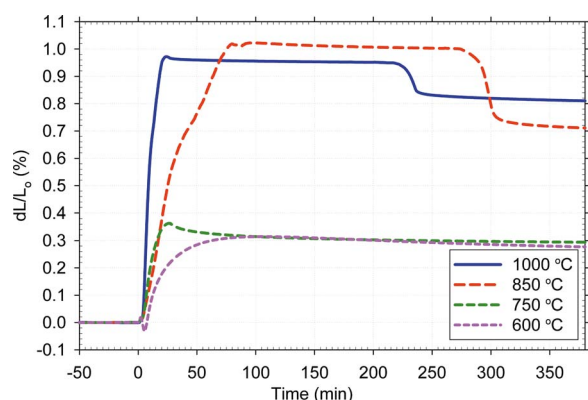
Figure 12. (Color online) Relative length change as a function of time for Ni–YSZ cermets all pre-reduced at 1000°C and reoxidized, at temperatures of 600, 750, 850, and 1000°C. The dL scale is shifted to zero prior to the reoxidation, and the reoxidation commences at $t = 0$. Two "domains" of behavior can be identified: less strain at low temperatures (600 and 750°C) and more strain at high temperatures (850 and 1000°C).
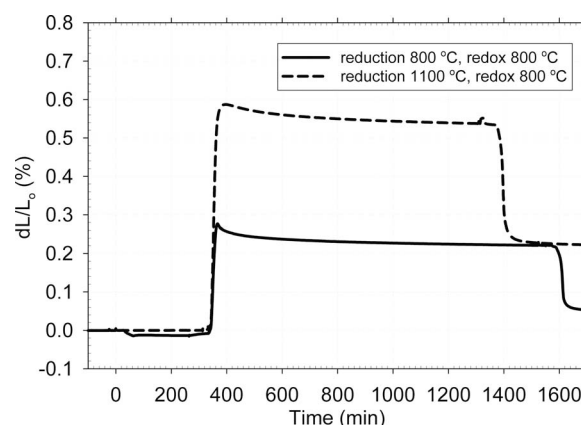

Figure 11. Relative length change vs time due to reoxidation of reduced Ni–YSZ composites showing the effect of the initial reduction temperature on redox strain. The solid line is for a cycle where both the reduction and reoxidation were done at 800°C, the dashed one showing reduction at 1100°C and redox at 800°C. Reoxidation commences at t ≈ 340 min, the zero point on the dL/L_o scale corresponds to the as-sintered hot state length (solid line) or hot state reduced length before reoxidation (dashed line).

this set of experiments mainly[e] related to differences in the thermomechanical behavior of the composites during the oxidation phase, including also possible effects from reaction kinetics depending on the temperature. Results from the cyclic redox dilatometry experiments with different reoxidation temperatures are given in Fig. 12. The time scale has been shifted so that the reoxidations commence at $t = 0$; thus, the initial reduction (not shown) takes place during negative time. The dL axis has been shifted to $dL/L_o = 0$ in reduced state at each temperature before the reoxidation. The maximum strains upon the reoxidation at different temperatures are given in Table II.

Data analysis.— We have used a systematic approach based on selected points directly derived from the isothermal dilatometry data in accordance with the practice used in Ref. 7 and 16. The CRS is tabulated for the following steps (see Fig. 1):

0. Initial relative length when the sample is kept isothermally in oxidized state ($dL/L_o = 0$).
1. Relative sample length shortly after reduction.
2. Relative sample length after a hold (here 12–18 h) under reducing conditions.
3. Maximum relative sample length after the first reoxidation.
4. Relaxed relative sample length at the end of the reoxidation step.
5. Relative sample length after the fast shrinkage of the sample upon the second reduction.
6. Relative sample length after a second reduction stabilization period.
7. Further numbers in the same manner for each point of interest in the dL curve up to three redox cycles.

We further define the parameter degree of redox reversibility (DRR) describing the strain reversibility during the redox cycles. DRR is based on the following quantities (Fig. 1): a = shrinkage of a sample in an oxidized state upon reduction (from the CRS_{msx} during the preceding oxidized state or redox cycle), and b = maximum expansion of a reduced sample upon reoxidation. The parameter DRR is defined as $DRR = a/b$ and describes the fraction of the reoxidation expansion that is recovered upon re-reduction; thus, a value of unity

would mean perfect strain reversibility during redox cycling. The values of parameters a and b were derived directly from the measurement data. The values of DRR were calculated for each redox cycle. In Ref. 16 further parameters were also defined, but a full analysis of those is not employed here. Table I shows the CRS_{max}, $CRS_{reduced}$, and DRR derived for the dry isothermal tests shown in Fig. 3, as well as the humid case displayed in Fig. 7. The strain reversibility during redox cycling is very close to unity at 600°C but decreases to about 0.8 at 800°C and is as low as about 0.17 at 1000°C. Introducing 6% humidity and a very high p_{H_2O}/p_{H_2} at 850°C decreases the DRR to 0.31–0.34, where the dry isothermal case had a DRR of 0.44–0.49.

Discussion

A number of dilatometry redox experiments have been carried out on porous Ni–YSZ composites under a wide range of operation conditions. First, the dimensional response to the initial reduction depending on the reduction temperature was studied as shown in Fig. 2 and Table I. The reduction of NiO to Ni results in an increase in porosity. In a system where the NiO/Ni and YSZ networks are interfacially well connected, the reduction shrinkage in the continuous NiO/Ni phase would transfer an internal contracting force onto the ceramic backbone. We suggest that how much of this phase change contraction can be measured in the bulk dimension of the composite depends on the interfacial and relaxation processes in the composite. The relaxation could be due to temperature-dependent processes such as elastic, anelastic, or plastic deformations (creep) in the components of the composite or interfacial effects between NiO, Ni, and YSZ, e.g., nickel sintering and dewetting. At low temperatures both the reaction kinetics and the relaxation processes are slower; a small part of the NiO → Ni contraction is transferred into the bulk dimension. At intermediate temperatures the relaxation is faster so that stresses largely relax while they are created by the reduction; thus, little or no length change was measured. As for the high-temperature reduction behavior, it is suggested that the shrink-

---

Table II. Relative length change of Ni-YSZ composite samples upon reoxidation at temperatures from 600 to 1000°C. All samples were pre-reduced at 1000°C before the redox cycle.

Temperature (°C)	600	750	850	1000
Strain on reoxidation, % dL/L_o (Fig. 12)	0.31	0.36	1.02	0.97

age of NiO to Ni during reduction exposes a new YSZ surface which can be active for sintering and thus, the sample shrinks due to sintering of the ceramic backbone when the temperature is high enough, in this case above 1000°C. The low-temperature contraction of the composite can hardly arise from residual stresses in the composite due to the difference in the coefficient of thermal expansion (CTE) of NiO and YSZ. The CTE is 1.41×10^{-5} K^{-1} for NiO and 1.03×10^{-5} K^{-1} for YSZ,[22] and there is an internal stress contracting the YSZ network after cooldown from high-temperature sintering and an unknown temperature of zero internal stress (depending on, e.g., the cooling rate). How fast the stress is relaxed is a function of time and temperature, but it is hardly possible that this stress would have relaxed and turned into a tensile force on the YSZ during the heat-up to 600°C prior to the initial reduction. Thus, we do not consider the relaxation of the internal thermal stress to be a plausible origin of the low-temperature contraction upon reduction.

The dimensional behavior on isothermal redox cycling was investigated under varying temperature and humidity conditions as summarized in Table I. From the reported redox cycling dilatometry, a clear dependency on temperature can be noted. The durations of the reduction-oxidation treatments were long enough at each step to either completely reduce or oxidize the samples. Even if the step durations between the different isothermal temperatures differ, we consider them valid for comparing the behavior between different isothermal temperatures. In other words, we think that the effect of the redox conditions is greater than that of the step durations. Increasing the temperature impairs redox stability by fast takeoff of the CRS far beyond the target level of maximum *CRS* = 0.1% set for the anode-supported SOFC (based on work reported in Ref. 13-15). However, not even at the lowest temperature tested does the tested material reach the target level. Second, when about 6% humidity was introduced during 2 h prior to each dry air reoxidation by mixing air, N_2, and H_2, the cumulative expansion after three redox cycles at 850°C increased almost 80% (from 1.55 to 2.78%, Table I). This is in qualitative agreement with literature suggesting enhancement of Ni sintering with humidity in microcomposites.[19,20] Sehested et al. examined the sintering of Ni nanocatalysts on Al_2O_3 support at 550°C and reports increased Ni particle growth with increasing p_{H_2O}/p_{H_2} ratio. He explains the increase in Ni sintering in the presence of humidity through the improved surface diffusivity of the Ni_2–OH species formed. It could thus be argued that the formation of the nickel hydroxide is favored by the increasing p_{H_2O}/p_{H_2} ratio.[3,4] If all the redox cycles are performed at 850°C in humid gas (log[p_{O_2}] between ≈ -2.8 and -2.3), redox expansion on the third reoxidation is slightly more than was measured at 1000°C and dry conditions. The p_{H_2O}/p_{H_2} ratios during all the experiments with humid gas were very high. For the steam–oxygen–hydrogen balance the situation is actually close to an operating cell with fully utilized fuel when the oxygen and hydrogen react close to stoichiometric ratios to produce H_2O. In our interpretation the increase in the redox strain observed at 850°C and humid conditions is a result of increased Ni sintering due to the presence of steam. The fact that at 600°C no such effect with humidity could be discerned suggests that the effect from steam is insufficient at that temperature to activate significant Ni sintering in the microcomposite studied.

From calculations using the thermodynamic code FACTSAGE, the oxidation–reduction equilibrium between Ni/NiO is roughly at $p_{O_2} \approx 6 \times 10^{-20}$, 10^{-13}, and 5×10^{-11} at temperatures of 600, 850, and 1000°C, respectively. In practice, the kinetics of the oxidation–reduction process depends, besides on the p_{O_2}, on the molar flow of oxygen per moles of nickel in the sample, arriving at the metal surface where the oxidation reaction takes place. In the redox tests in dry air, the incoming $p_{O_2} = 0.2$ and the theoretical reoxidation times, if all oxygen supplied would be consumed in oxidizing nickel, are about 1–3 min. In humid or wet conditions this situation changes drastically, because the measured p_{O_2} is then about 10^{-2}–10^{-4} and furthermore, the oxidation reaction is likely to also involve intermediate species such as the Ni_2–OH. As a result, some-

what slower oxidation kinetics could be expected under humidified conditions and the same total gas flow. Differences in oxidation kinetics could indeed be indirectly observed in the measurements by comparing the rates of expansion of the tests with humid gas in Fig. 8 and 9. Some signs of reoxidation at 850°C were observed at $p_{O_2} \approx 5 \times 10^{-12}$ (about 2300–2600 min into the test) in Fig. 8. It is likely that some oxidation of the Ni took place, but since the kinetics were slow, it did not yet reflect in sample dimension; for measurable redox strains a relatively large fraction of the Ni needs to be oxidized before the composite shows oxidation strain. The subsequent redox cycle (starting at $t \approx 2800$ min) up to $p_{O_2} \approx 10^{-3}$ clearly reoxidized the sample, but with slower kinetics [reduced slope d/dt(dL/L)%/min] than what was observed in Fig. 7. The last reoxidation in Fig. 8 (starting at about $t \approx 3750$ min) suggests faster oxidation kinetics, which is reflected by a steeper slope of the expansion curve. Similar increase in the expansion rate could be observed in Fig. 9, where the measured log[p_{O_2}] values during the three first reoxidations were about -2.8, -2.5, and -2.3, respectively. The fourth reoxidation was carried out in dry air and showed by far the fastest expansion. The amount of oxygen in the test chamber was thus reflected in the slope of oxidation strain, showing differences in oxidation kinetics. During low-temperature redox cycling (Fig. 10), the four first reoxidations of about 10 h duration each did not bring the sample to dimensional stability apparently due to slow kinetics. The first clear redox strain starts on the second p_{O_2} increase at log[p_{O_2}] ≈ -2.5 ($t \approx 2700$ min). The sixth reoxidation was longer (about 33 h) and there the maximum CRS measured was 0.21% dL/L.

The effect of the initial reduction temperature was investigated by reducing cermets at a high temperature (1100°C) and an intermediate temperature (800°C) and reoxidizing them both at 800°C (Fig. 11). The initial reduction carried out at a high temperature more than doubled the redox expansion. It is reasonable to assume that the degree of Ni sintering (the growth of Ni grains) is dependent on temperature, and according to the model of redox instability,[5,12] this reflects in the bulk redox strain upon reoxidation, in this case by a factor of about 2.

In this work we have shown that the effect of reoxidation temperature is equally important for redox behavior. Four samples were pre-reduced at 1000°C and reoxidized at different temperatures. The samples reoxidized at 850 and 1000°C show roughly 1% expansion on the first reoxidation, whereas reoxidation at 750 or 600°C reduces the redox strain to approximately one-third (0.36 and 0.31% dL/L$_o$ for the two temperatures, respectively). These results thus suggest that the relative importance on the total redox strain from the reoxidation temperature is equal to or larger than the effect from initial reduction temperature or the degree of Ni sintering prior to the reoxidation. Reoxidation taking place at a low temperature involves a mechanism that reduces the redox strain by removing a part of the reoxidation stress exerted by the Ni/NiO phase on the YSZ backbone. This stress relaxation during the oxidation phase is not yet fully understood but is likely to be connected with microstructural changes in the composite due to redox cycling, or changes in the reaction kinetics. Possible relaxation processes could be deformation, cracking, or relocation of the oxidizing Ni grains, or possibly also Ni–YSZ interfaces. Also, the partially stabilized zirconia used in the cermet is stronger at lower temperatures, where the hardening martensitic transformation from the tetragonal to the monoclinic phase is easier to achieve.

From Tables I and II it can be observed that both increase in temperature and humidity (at high temperatures) reduce redox reversibility, i.e., the fraction of the reoxidation strain that is recovered on re-reduction of the composite. The reoxidation of nickel results in a large tensile stress in the load-bearing YSZ network. Irreversible permanent deformations of YSZ can occur, e.g., by cracking or by plastic deformation (creep or grain boundary sliding) at high temperatures. The amount of expansion upon reoxidation could be taken as a measure of the irreversible Ni coarsening minus the effect of

stress deduction during the reoxidation phase. The DRR is thought to be connected with the amount of micro- and macrodamage as well as creep in the YSZ. Once the ceramic YSZ backbone is fractured due to excessive stress caused by the reoxidation strain, its capability to return to the original dimension is degraded. The very small values of DRR at 1000°C suggest that fractures in the YSZ network have occurred to accommodate the oxidation strain.

Conclusions

Ni–YSZ cermets of the type used for SOFC were tested in redox cycling dilatometry under a wide range of operation conditions. The main parameters that were varied were temperature and humidity. Dependencies of the dimensional behavior of the cermet were obtained both during reduction and reoxidation.

Upon initial reduction at low temperatures (600°C), a contraction of about 0.08% and recovery toward the initial length was observed. At intermediate temperatures (800–850°C), little or no dimensional change was measured upon reduction. Upon reduction at high temperature (1000°C), bulk shrinkage of 0.05% after was measured; at still higher temperatures the cermet shows marked shrinkage upon reduction.

Cumulative redox strain after three redox cycles in dry conditions increases from 0.25 to 3.2% dL/L_o, when the isothermal redox cycling temperature is lifted from 600 to 1000°C. Humidity deteriorates redox stability at high temperatures (roughly 850°C or above); CRS after three redox cycles under 6% steam and a very high p_{H_2O}/p_{H_2} ratio was in one case slightly less and in another case in excess of the CRS from dry redox cycling at 1000°C. No effect on redox strain by humidity was observed at 600°C. The degree of reversibility of the redox strain decreases with increasing temperature and at 850°C in the presence of humidity. The rate of dimensional change during oxidation decreased when p_{O_2} during the oxidation phase decreased.

It was confirmed that Ni sintering deteriorates redox stability by increasing redox strain on reoxidation. Of two similar samples, one was reduced 5.5 h at 800°C and the second one 4.5 h at 1100°C. The sample reduced at 1100°C showed about twice the amount of redox strain when reoxidized at 800°C.

It was found that the temperature of reoxidation is an important parameter affecting the total redox strain. In samples pre-reduced 3 h at 1000°C the reoxidation strain was about 1% when reoxidation took place at 850 or 1000°C, whereas it was 0.31–0.36% when the reoxidation was carried out at 600 or 750°C. In the investigated data set, the temperature of reoxidation actually played a bigger role than the temperature of the initial reduction.

References

1. N. Minh, *J. Am. Ceram. Soc.*, **3**, 563 (1993).
2. D. Simwonis, F. Tietz, and D. Stöver, *Solid State Ionics*, **132**, 241 (2000).
3. J. Sehested, J. A. P. Gelten, I. N. Remediakis, H. Bengaard, and J. K. Nørskov, *J. Catal.*, **223**, 432 (2004).
4. J. Sehested, J. A. P. Gelten, and S. Helveg, *Appl. Catal., A*, **309**, 237 (2006).
5. T. Klemensø, C. Chung, P. H. Larsen, and M. Mogensen, *J. Electrochem. Soc.*, **152**, A2186 (2005).
6. D. Sarantaridis and A. Atkinson, *Fuel Cells* **7**, 246 (2007).
7. G. Robert, A. Kaiser, and E. Batawi, in *Proceedings of the 6th European SOFC Forum*, European Fuel Cell Forum, p. 193 (2004).
8. D. Waldbillig, A. Wood, and D. G. Ivey, *Solid State Ionics*, **176**, 847 (2005).
9. J. Malzbender, E. Wessler, and R. W. Steinbrech, *Solid State Ionics*, **176**, 2201 (2005).
10. M. Ettler, G. Blaß, and N. H. Menzler, *Fuel Cells* **7**, 349 (2007).
11. D. Sarantaridis, R. A. Rudkin, and A. Atkinson, *ECS Trans.*, **7**(1), 1491 (2007).
12. T. Klemensø and M. Mogensen, *J. Am. Ceram. Soc.*, **90**, 3582 (2007).
13. T. Klemensø, Ph.D. Thesis, Technical University of Denmark (2005).
14. D. Sarantaridis and A. Atkinson, in *Proceedings of the 7th European SOFC Forum*, European Fuel Cell Forum, Paper P0728 (2006).
15. J. Laurencin, G. Delette, F. Lefebvre-Joud, and M. Dupeux, *J. Eur. Ceram. Soc.*, **28**, 1857 (2008).
16. M. Pihlatie, A. Kaiser, P. H. Larsen, and M. Mogensen, *ECS Trans.*, **7**(1), 1501 (2007).
17. N. Christiansen, J. B. Hansen, H. Holm-Larsen, S. Linderoth, P. H. Larsen, P. V. Hendriksen, and M. Mogensen, in *Proceedings of the 7th European SOFC Forum*, Paper B034 (2006).
18. S. Ramousse, M. Menon, K. Brodersen, J. Knudsen, U. Rahbek, and P. H. Larsen, *ECS Trans.*, **7**(1), 317 (2007).
19. K. Thydén, R. Barfod, and Y. Liu, *Adv. Sci. Technol. (Faenza, Italy)*, **45**, 1483 (2006).
20. S. P. Jiang, *J. Mater. Sci.*, **38**, 3775 (2003).
21. R. Haugsrud, *Corros. Sci.*, **45**, 211 (2003).
22. M. Mori, T. Yamamoto, H. Itoh, H. Inaba, and H. Tagawa, *J. Electrochem. Soc.*, **145**, 1374 (1998).